Reflective point-diffraction microscopic interferometer with long-term stability

(Invited Paper)

Rongli Guo (郭荣礼)[1,2], Baoli Yao (姚保利)[1*], Peng Gao (郜 鹏)[1], Junwei Min (闵俊伟)[1], Juanjuan Zheng (郑娟娟)[1], and Tong Ye (叶 彤)[1]

[1]*State Key Laboratory of Transient Optics and Photonics, Xi'an Institute of Optics and Precision Mechanics, Chinese Academy of Sciences, Xi'an 710119, China*

[2]*Graduate University of Chinese Academy of Sciences, Beijing 100049, China*

[*]*Corresponding author: yaobl@opt.ac.cn*

Received August 1, 2011; accepted November 18, 2011; posted online November 30, 2011

An on-axis phase-shifting reflective point-diffraction microscopic interferometer for quantitative phase microscopy based on Michelson architecture is proposed. A cube beamsplitter splits the object wave spectrum into two copies within two arms. Reference wave is rebuilt in one arm by low-pass filtering on the object wave frequency spectrum with a pinhole-mask mirror, and interferes with the object wave from the other arm. Polarization phase-shifting is performed and phase imaging on microscale specimens is implemented. The experimental results demonstrate that the proposed scheme has the advantage of long-term stability due to its quasi common-path geometry with full use of laser energy.

OCIS codes: 090.2880, 180.3170, 120.3180, 120.5050.
doi: 10.3788/COL201109.120002.

Visualization and characterization of transparent objects, such as biological features and microlens arrays, are highly demanding in various disciplines. Interferometric technique is a non-invasive high-resolution whole-field technique for measuring such transparent specimens[1−9]. However, most interferometers have widely-separated object beam path and reference beam path, therefore, are sensitive to environmental disturbance. Thus, if no proper precautions are taken, the fringe pattern in the observation plane is unstable[10]. To increase stability of system, common-path configuration is often adopted. Phase contrast method[11] provides a qualitative investigation of phase objects, which converts phase distribution arising from both refractive index and sample thickness into intensity contrast. Popescu *et al.* proposed an off-axis point-diffraction interferometric (PDI) technique and developed a diffraction phase microscope[12,13]. Ding *et al.* improved this method by using white light illumination to eliminate coherent noise[14]. The microscope has advantage of one-shot recording and is suitable for investigating dynamics process of cells. In the other side, they cannot make full use of lateral resolution of charge-coupled device (CCD) due to its off-axis geometry. To overcome this drawback, on-axis geometry with phase-shifting mechanism is the best choice. Mercer *et al.* applied phase-shifting technique to point-diffraction interferometry with a liquid-crystal[15]. Iemmi *et al.* applied a liquid crystal television display to PDI for holography[16]. However, when a phase modulator is adopted, fringe contrast cannot be changed, and in the meantime the light efficiency is decreased as multiple diffraction orders created due to its pixilated structure. Kadono *et al.* implemented polarization phase-shifting technique in PDI with a series of polarization elements, while, the phase-shift between object and reference beams is nonlinear, thus rotation angle of half-wave plate must be carefully selected[17]. Neal *et al.* proposed a PDI configuration, which adopted a birefringent pinhole plate for phase-shifting[18]. Wang *et al.* used a semi-transmitting pinhole mirror to produce reference wave in PDI[19]. In these two cases, both pinhole plate and pinhole mirror need sophisticated fabrication, which in turn increased the cost of system.

Recently, on-axis phase-shifting PDI has been developed in our group by using a pair of gratings[20]. However, more than 50% of laser energy is wasted since two gratings are employed and half diffraction orders are used. Besides, light sources with broad spectrum cannot be used in that configuration due to the dispersion of the gratings. In this letter, we present a new on-axis phase-shifting PDI based on a Michelson configuration. This configuration has the advantage of long-term stability due to its quasi common-path geometry with full use of laser energy. In addition, both split object waves propagate along on-axis, which brings convenience for pinhole filtering and provides the possibility of using light sources with broad spectrum to depress the coherent noise.

The experimental setup of the proposed polarization phase-shifting PDI for microscopy is depicted in Fig. 1. A randomly polarized He-Ne laser with wavelength of 632.8 nm is used as light source. A neutral variable attenuator NF is located on the output laser beam to adjust the intensity. The linear polarizer P_1 has a polarization angle θ with respect to horizontal direction. The laser beam becomes linearly polarized when passing through P_1 and then is expanded and collimated by the beam expander BE. The uniform beam illuminates the specimen which locates in the front focal plane of microscopic objective MO. After passing through the specimen, the object wave is magnified by the objective MO, and collimated by lens L_1, thus the magnified image appears

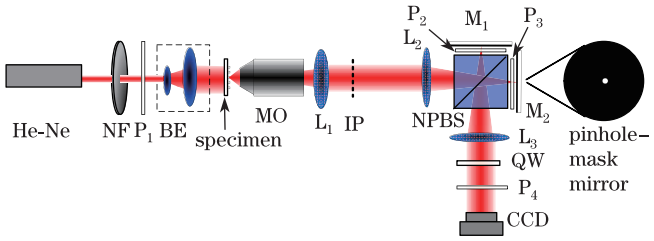

Fig. 1. Experimental setup. L_1−L_3, achromatic lenses with focal lengths of f_1=90 mm and $f_2 = f_3$=300 mm.

in the image plane IP. The image is Fourier-transformed by lens L_2 and the frequency spectrum is split by the non-polarizing beamsplitter (NPBS) into two copies, saying a reflected copy and a transmitted copy. Mirrors M_1 and M_2 locate at the focal planes of lenses L_3 and L_2, respectively. The reflected copy is directly reflected by M_1 and still serves as object wave, whereas the transmitted copy is filtered by a 20-μm-diameter pinhole-mask mirror M_2 to produce a spherical reference wave. Polarizers P_2 and P_3 with the horizontal and vertical polarizations are respectively located in the two arms, transforming the polarizations of the two waves into perpendicular polarizations. The two waves are combined by NPBS and Fourier-transformed by lens L_3. Since the normals of the two mirrors coincide with the optical axis, the reflected two beams propagate on-axis again. The complex amplitude of the object wave and the reference wave behind lens L_3 can be respectively expressed as

$$\begin{aligned} O &= \mathrm{IFT}\{\mathrm{FT}\{\tau_\mathrm{r} O_\mathrm{test}\}\tau_\mathrm{t}\cos\theta\}\cdot\begin{bmatrix}1\\0\end{bmatrix}, \\ R &= \mathrm{IFT}\{\mathrm{FT}\{\tau_\mathrm{t} O_\mathrm{test}\}T_\mathrm{PH}\tau_\mathrm{r}\sin\theta\}\cdot\begin{bmatrix}0\\1\end{bmatrix}, \end{aligned} \tag{1}$$

where O_test denotes the complex transmittance of the tested object, τ_r and τ_t denote the reflectance and transmittance coefficients of NPBS, T_PH denotes the transmittance of the pinhole-mask mirror, and FT{} and IFT{} denote the Fourier transformation and inverse Fourier transformation operations. A quarter-wave (QW) plate is placed behind the L_3, which has its fast axis at $\pi/4$ with respect to the horizontal direction to convert the perpendicularly linearly polarized object and reference waves into perpendicularly circular polarizations. The polarizer P_4 with its polarization angle α with respect to the horizontal direction is located in front of the CCD camera. According to the polarization phase-shifting analysis[21], the interferogram formed by the object and reference waves in the CCD plane can be written as

$$\begin{aligned} I(x,y) = {} & |O_0|^2\cos^2\theta + |R_0|^2\sin^2\theta \\ & + |O_0|\,|R_0|\sin 2\theta\sin[\varphi(x,y)+2\alpha], \end{aligned} \tag{2}$$

where O_0=$\tau_\mathrm{r}\tau_\mathrm{t}O_\mathrm{test}$ and R_0=$\tau_\mathrm{r}\tau_\mathrm{t}$ IFT{FT{O_test}T_PH} denote the complex amplitude of the object and reference waves; $\varphi(x, y)$ denotes the phase difference between the object and reference waves, which comprises two parts, i.e., specimen phase $\varphi_\mathrm{test}(x, y)$ and the background phase $\varphi_\mathrm{back}(x, y)$.

The fringe contrast is adjusted by rotating the polarization angle θ of the polarizer P_1, and the phase-shift in the interferograms can be introduced by rotating polarizer P_4. When the polarizer P_4 rotates an angle δ, the phase-shift of φ_s=2δ is obtained. Here, we rotate P_4 with an angle increment $\delta = \pi/4$ from initial angle α_0, and four interferograms with phase-shift of $\pi/2$ are acquired sequentially. The wrapped object phase $\varphi_\mathrm{wr}(x, y)$ is retrieved by using four-step reconstruction algorithm and unwrapped to generate phase distribution $\varphi(x, y)$[22]. The background phase distribution φ_back has been measured in advance without the specimen and the final unwrapped phase $\varphi_\mathrm{test}(x, y)$=$\varphi(x, y) - \varphi_\mathrm{back}(x, y)$ is obtained. Besides, a two-step phase-shifting technique[23,24] can also be applied as reference wave was measured in advance.

In the proposed configuration, the object and reference waves propagate in quasi common-path geometry, since mirrors M_1 and M_2 are placed as close as possible to NPBS. Therefore, the interferometer is insensitive to turbulences of the environment. In our experiment, the pinhole-mask mirror M_2 is prepared by attaching a pinhole filter to a mirror, which is fabricated on a stainless steel plate. The requirement on pinhole size in this configuration is not as strict as that in optical surface testing method[18] where a small enough pinhole is employed to produce ideally spherical reference wave, because even the reference wave has slight aberrations, it can be subtracted in the measurement.

We demonstrate the proposed configuration by measuring a micro-fabricated phase-step. The phase-step, which was etched in fused silica, has a rectangular shape of 70×20 (μm). The microscope objective MO has magnification of 40× and numerical aperture (NA) of 0.65. The total magnification of the setup is M=31.5, which is determined by the MO paired with the relay lens L_1. The CCD camera has 1048 (H)×768 (V) pixels with pixel size of 4.65 μm (H)×4.65 μm (V). By rotating the polarizer P_4 with increment of $\pi/4$, the phase-shifted interferograms were acquired and shown in Fig. 2.

After subtracting the background phase, the final phase distribution of the specimen is shown in Fig. 3(a), which provides a quantitative vision for the structure. The measured optical path difference (OPD) $\lambda\varphi_\mathrm{test}/2\pi$ of the phase-step is consistent with the real value. The OPD between the marked point A and the background is 162 nm, which agrees well with the expected value of 158 nm. The uncertainty may come from the fabrication error and the phase-shifting error. In order to evaluate the accuracy of the measurement, the phase along a cut-line

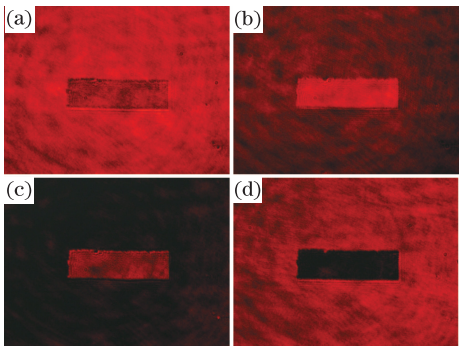

Fig. 2. Phase-shifted interferograms of the phase-step with phase-shifts of (a) 0, (b) $\pi/2$, (c) π, and (d) $3\pi/2$.

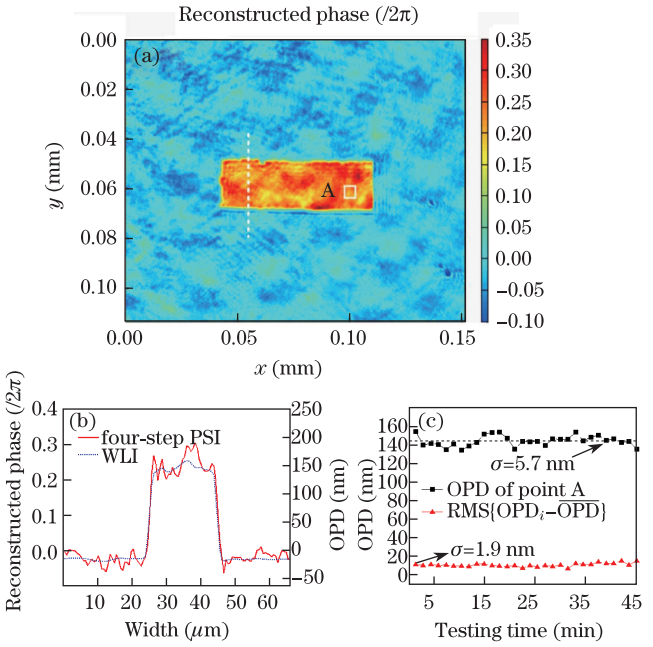

Fig. 3. Experimental results. (a) Final reconstructed phase profile of the tested phase step; (b) phase distribution as well as OPD along the cut line in (a); (c) stability test for the proposed setup.

crossing the specimen is extracted and compared with that obtained by the white light interferometer (WLI) (Talysurf CCI 6000, Taylor Hobson Inc., England). Figure 3(b) shows the reconstructed phase along the cut-line as well as the OPD. It can be seen that the measurement result is consistent well with that of WLI.

To quantify the stability of the proposed setup against the environmental disturbance, we repeatedly measured the phase-step 30 times within a period of 45 min at intervals of 1.5 min. The stability is assessed with temporal OPD fluctuation in the marked point A in Fig. 3(a). The fluctuation associated with point A is shown in Fig. 3(c). The phase of the point was averaged over an area of 0.6×0.6 (μm), which corresponded to the transverse resolution of the microscope. The standard deviation of the fluctuation is 5.7 nm, which means that the setup has long-term OPD stability. Besides, for evaluating the spatial fluctuations of OPD over the whole field of view, we calculated the root mean square (RMS) of the OPD between the reconstructed $\mathrm{OPD}_i (i = 1, 2, \cdots, 30)$ and the average $\overline{\mathrm{OPD}}$, as shown with triangle in Fig. 3(c). The average value of $\mathrm{RMS}\{\mathrm{OPD}_i - \overline{\mathrm{OPD}}\}$ is 10.3 nm. The repeatability, which is defined as the temporal standard deviation on the $\mathrm{RMS}\{\mathrm{OPD}_i - \overline{\mathrm{OPD}}\}$, is 1.9 nm (equivalent to $\lambda/330$). It means that the repeatability of the setup is high. The high stability and repeatability attribute to the quasi common-path configuration of the setup. As coherent light brings inevitably speckle noise in the experiment, we believe that the performance of system can be improved further by using low coherent light source.

In conclusion, we demonstrate a simple reflective point-diffraction interferometry for phase microscopy, which provides a non-perturbation means for measuring the phase images of microscopic objects. In this approach, the object wave is Fourier-transformed and split into two separated copies. One is low-pass filtered by a pinhole-mask mirror and used as the reference wave, while the other keeps unchanged and still behaves as the object wave. With the help of polarization elements, phase-shifting interferometry can be implemented. Owing to its on-axis quasi common-path configuration, the proposed method has high lateral resolution and high temporal stability. This feature makes it suitable for phase imaging over periods of hours. In the same time, it can make full use of laser energy. Moreover, the system can be used for two-wavelength point-diffraction interferometry, allowing one to extend the axial dynamic measurement range.

This work was supported by the National Natural Science Foundation of China under Grant Nos. 61077005, 61107003, and 10874240.

References

1. I. Yamaguchi, J. Kato, S. Ohta, and J. Mizuno, Appl. Opt. **40,** 6177 (2001).
2. Y. X. Wang, D. Y. Wang, J. Zhao, Y. S. Yang, X. Q. Xiao, and H. K. Cui, Chin. Opt. Lett. **9,** 030901 (2011).
3. F. Charrière, J. Kühn, T. Colomb, F. Montfort, E. Cuche, Y. Emery, K. Weible, P. Marquet, and C. Depeursinge, Appl. Opt. **45,** 829 (2006).
4. B. Kemper and G. V. Bally, Appl. Opt. **47,** A52 (2008).
5. C. J. Mann, L. Yu, C.-M. Lo, and M. K. Kim, Opt. Express **13,** 8693 (2005).
6. W. J. Qu, C. O. Choo, V. R. Singh, Y. J. Yu, and A. Asundi, Appl. Opt. **49,** 6448 (2010).
7. P. Marquet, B. Rappaz, P. J. Magistretti, E. Cuche, Y. Emery, T. Colomb, and C. Depeursinge, Opt. Lett. **30,** 468 (2005).
8. M. T. Rinehart, N. T. Shaked, N. J. Jenness, R. L. Clark, and A. Wax, Opt. Lett. **35,** 2612 (2010).
9. T. Ikeda, G. Popescu, R. R. Dasari, and M. S. Feld, Opt. Lett. **30,** 1165 (2005).
10. D. Malacara, *Optical Shop Testing* (3rd edn.) (Wiley, Hoboken, 2007).
11. F. Zernike, Science **121,** 345 (1955).
12. G. Popescu, T. Ikeda, R. R. Dasari, and M. S. Feld, Opt. Lett. **31,** 775 (2006).
13. Y. Park, G. Popescu, K. Badizadegan, R. R. Dasari, and M. S. Feld, Opt. Express **14,** 8263 (2006).
14. H. Ding and G. Popescu, Opt. Express **18,** 1569 (2010).
15. C. Mercer and K. Creath, Opt. Lett. **19,** 916 (1994).
16. C. Iemmi, A. Moreno, and J. Campos, Opt. Express **13,** 1885 (2005).
17. H. Kadono, T. Nobukatsu, and T. Asakura, Appl. Opt. **26,** 898 (1987).
18. R. M. Neal and J. C. Wyant, Appl. Opt. **35,** 3463 (2006).
19. D. Wang, Y. Yang, C. Chen, and Y. Zhuo, Appl. Opt. **50,** 2342 (2011).
20. P. Gao, I. Harder, V. Nercissian, K. Mantel, and B. Yao, Opt. Lett. **35,** 712 (2010).
21. G. Rodriguez-Zurita, C. Meneses-Fabian, N. Toto-Arellano, J. Vazquez-Castillo, and C. Robledo-Sánchez, Opt. Express **16,** 7806 (2008).
22. M. A. Herraez, D. R. Burton, M. J. Lalor, and D. B. Clegg, Appl. Opt. **35,** 5847 (1996).
23. X. F. Meng, L. Z. Cai, X. F. Xu, X. L. Yang, X. X. Shen, G. Y. Dong, and Y. R. Wang, Opt. Lett. **31,** 1414 (2006).
24. J.-P. Liu and T.-C. Poon, Opt. Lett. **34,** 250 (2009).